Accepted to *Applied Spectroscopy* In press (2016)

Analytical and Numerical Characterization of Autocorrelation and Perturbation-Correlation Moving-Window Methods

Young Jong Lee*

Biosystems and Biomaterials Division, National Institute of Standards and Technology, Gaithersburg, MD 20899, USA

Abstract

Moving-window (MW) approaches to two-dimensional correlation spectroscopy make it possible to characterize spectral changes occurring in a narrow range of perturbation variable (e.g., time, temperature, and concentration). Despite the wide range of application, the physical meanings of MW correlation intensities have been only qualitatively associated with the direction and curvature of spectral intensity change with respect to a perturbation variable. Here are full and simplified analytical expressions of autocorrelation moving-window (AC-MW) and synchronous and asynchronous perturbation-correlation moving-window (*s*-PC-MW and *as*-PC-MW) intensities. When the window is set sufficiently narrower than the bandwidth of spectral change, the square root of AC-MW intensity and *s*-PC-MW intensity becomes proportional to the first order derivative, and *as*-PC-MW intensity becomes proportional to the negative of the second order derivative. This paper demonstrates that both AC-MW and PC-MW profiles can be significantly altered by non-uniform perturbation spacing. It is also found that intensity noise can cause AC-MW to display a false offset drift. This analytical and numerical characterization of the two MW correlation intensities elucidates their physical meanings and ascertains the analysis conditions for reliable interpretation.

1. Introduction

Since generalized two-dimensional correlation spectroscopy (2DCOS) was introduced by Noda,[1] the method has been widely used to analyze spectral data acquired as a function of perturbation variables such as temperature, pressure, time, and concentration.[2] The synchronous and asynchronous correlation spectra generated by 2DCOS are used to determine the directions and sequences of the spectral changes and to resolve underlying spectral bands. However, when multiple changes occur within the perturbation range of a 2DCOS analysis, the correlation spectra involve mixed contributions of the different changes and it becomes difficult to interpret their physical meanings from the complex correlation results.

The moving-window (MW) approach, first introduced to 2DCOS in 2000 by Thomas and Richardson,[3] can alleviate this complication by partitioning and moving the perturbation variable range (window) of 2DCOS analysis. For example, the autocorrelation spectrum is used to represent the spectral intensity change as a function of the average perturbation variable. An autocorrelation peak spectrum is obtained from the diagonal line in a synchronous 2D correlation map, which indicates the overall extent of spectral intensity variation within a perturbation variable range. A 1D autocorrelation spectrum can be consecutively calculated from each window as a function of the average perturbation variable. The resulting autocorrelation moving-window (AC-MW) spectra are displayed as a 2D contour map or a waterfall plot, which is useful for visualizing the spectral change over the entire perturbation range and to determine the perturbation values where phase transitions and chemical reactions are occurring in polymers,[4,5] liquid crystals,[3] hydrogels,[6] and proteins.[7,8]

Later in 2003, Morita et al.[9] proposed a new MW method, called as perturbation-correlation moving-window (PC-MW), which calculates the correlation between the perturbation variable and the spectral intensity of each spectral variable. Similar to the generalized 2DCOS, PC-MW generates synchronous and asynchronous correlation spectra, which represent the (in-phase) direction and the (out-of-phase) curvature of spectral intensity change, respectively. Unlike AC-MW, synchronous PC-MW maps provide not only the degree of correlation of intensity change between multiple spectral components, but also the direction; therefore, they have become a widely used MW method in various applications.[10–17] Jung et al.[18] demonstrated that a 2D gradient map can locate physical and chemical transitions by calculating intensity difference over each perturbation step. However, noise amplification associated with differentiation typically requires additional pre- or post-processes for denoising. Morita et al.[19] demonstrated that AC-MW intensity shows a higher signal-to-noise ratio than the square of a gradient map even after the gradient map is smoothed by the Savitzky-Golay smoothing with the same window size with the AC-MW.

Interpretations of AC-MW and PC-MW intensities are related to the first and second order derivatives of spectral intensity along the perturbation variable. Morita et al.,[19] used a simple three-point model to propose that AC-MW intensity is proportional to the square of the first order derivative of spectral intensity, which was supported by the similarity between the shape of the calculated AC-MW intensity and the shape of the square of the first order derivative of simulation data. Morita et al.[9] used the same three-point model and simulation data to prove that the synchronous PC-MW (*s*-PC-MW) intensity is proportional to the first order derivative. They also asserted that the

asynchronous PC-MW (*as*-PC-MW) intensity is proportional to the negative of the second order derivative by comparing the general trends of *as*-PC-MW profiles calculated from simulation data with the derivative of the corresponding *s*-PC-MW profiles. Other reports on the physical interpretations of AC-MW and PC-MW results[15,20–22] are also based on comparison of simulated MW correlation results and the model function. However, the connection between MW correlation intensity and the first or second order derivative has never been mathematically derived using analytical expressions. The absence of analytical description makes it challenging to quantitatively validate the proportionality between MW correlation intensity and the first or second order derivative and to characterize their associated limiting conditions.

Here is an analytical description of the AC-MW and PC-MW correlation intensities with a continuous model intensity function. The description helps to understand the mathematical connections between the correlation intensities and the first/second derivatives of spectral intensity. Then, a numerical description for discrete forms of spectral data is presented to discuss the effect of the moving-window size, non-uniform perturbation increment, and intensity noise of the MW correlation results.

2. Analytical Descriptions of Moving-Window Correlation Spectroscopy

2.1 2D Correlation Spectroscopy and its Moving-Window Approach

The generalized 2DCOS analyzes a series of spectra, $y(\nu, p)$ acquired as a function of spectral variable ν (typically in wavelength or frequency) and external perturbation variable p (typically in time, pressure, temperature, or concentration). 2DCOS yields a complex correlation spectrum between a pair of spectral variables, where the real term is

called the synchronous correlation spectrum, Φ, and the imaginary term is called the asynchronous correlation spectrum, Ψ:

$$\Phi(\nu_1,\nu_2) + i\Psi(\nu_1,\nu_2) = \frac{1}{\pi(p_{max}-p_{min})}\int_0^{\infty}\tilde{Y}_1(\omega)\tilde{Y}_2^*(\omega)d\omega \quad (1)$$

where

$$\tilde{Y}_1(\omega) = \int_{-\infty}^{\infty}\tilde{y}(\nu_1,p)e^{-i\omega p}dp \quad (2)$$

and

$$\tilde{Y}_2^*(\omega) = \int_{-\infty}^{\infty}\tilde{y}(\nu_2,p)e^{+i\omega p}dp \quad (3)$$

are the Fourier transforms of the mean-centered spectrum, $\tilde{y}(\nu,p)$, also known as the dynamic spectrum defined as,

$$\tilde{y}(\nu,p) = \begin{cases} y(\nu,p) - \bar{y}(\nu), & p_{min} < p < p_{max} \\ 0 & , otherwise \end{cases} \quad (4)$$

$\bar{y}(\nu)$ is the reference spectrum, typically defined as the average spectrum over $p_{min} < p < p_{max}$. Intensity of a synchronous 2D correlation spectrum represents the simultaneous or coincidental changes of two spectral intensities while that of an asynchronous 2D correlation spectrum represents sequential or successive changes of them.

In 2000, Noda demonstrated that a new algorithm can simplify calculation of the synchronous and asynchronous correlation spectra without using Fourier transformation.[23] He showed that the synchronous and asynchronous 2D correlation spectra can be expressed as

$$\Phi(\nu_1,\nu_2) = \frac{1}{(p_{max}-p_{min})}\int_{p_{min}}^{p_{max}}\tilde{y}(\nu_1,p)\tilde{y}(\nu_2,p)dp \quad (5)$$

$$\Psi(\nu_1,\nu_2) = \frac{1}{(p_{max}-p_{min})}\int_{p_{min}}^{p_{max}}\tilde{y}(\nu_1,p)\tilde{z}(\nu_2,p)dp \quad (6)$$

where $\tilde{z}(\nu_2,p)$ is the orthogonal spectrum of $\tilde{y}(\nu_2,p)$ converted by Hilbert transformation as

$$\tilde{z}(\nu_2, p) = \mathcal{H}[\tilde{y}(\nu_2, p)] = \frac{1}{\pi} PV \int_{-\infty}^{\infty} \frac{\tilde{y}(\nu_2, p')}{p' - p} dp' \tag{7}$$

The "$PV\int$" denotes that the Cauchy principal value is taken to exclude the singularity. I find that these expressions are quite useful to analyze both analytical (continuous) and discrete forms of spectral data and to understand differences in the characteristics of different 2DCOS methods.

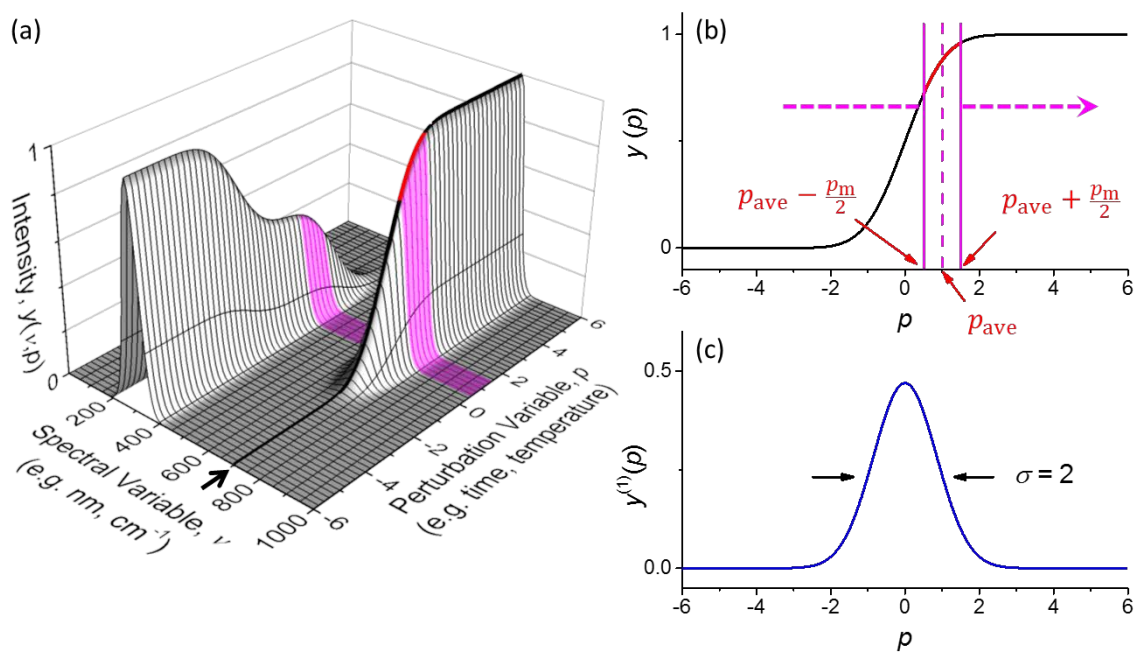

Figure 1. (a) Illustration of a moving-window analysis for a series of spectra, $y(\nu, p)$, where ν is the spectral variable and p is the perturbation variables. At a specific spectral variable, the intensity, $y(p)$, is analyzed as a function of p. (b) The intensity is plotted at $\nu = 700$, which is simulated with Eq. 8 with the center $p_c = 0$ and the FWHM $\sigma = 2$. The moving-window (denoted as the magenta region) is described by the average perturbation value, p_{ave}, and the width of p_m. (c) The first order derivative, $y^{(1)}(p)$, of the intensity in (b) is plotted.

The basic concept of moving-window (MW) correlation spectroscopy has been explained elsewhere.[4,9,19] Briefly, as illustrated in Figure 1a, a large set of spectral data is partitioned by a small subset or window, a 2D correlation spectrum of the window is

obtained, and the analysis is repeated for shifted or moved windows. Here, I discuss different 2DCOS methods applied to the moving window analysis and compare their results from model functions. Figure 1b shows a model spectral intensity function, $y(p)$, and an example of a moving window within the range of $p_{\mathrm{ave}} - \frac{p_{\mathrm{m}}}{2} < p < p_{\mathrm{ave}} + \frac{p_{\mathrm{m}}}{2}$, where p_{ave} is the average perturbation value and p_{m} is the window size. For $\tilde{y}(\nu, p) = I(\nu)\tilde{y}(p)$, this paper will focus on only $y(p)$ by treating $I(\nu)$ as a constant. The model function used for $y(p)$ is a modified error function, which represents the integral form of a Gaussian function with the center at p_{c} and the full-width-half-maximum (FWHM) of σ.

$$y(p) = \frac{1}{2}\mathrm{erfc}\left[-2\sqrt{\mathrm{Ln}\,2}\,\left(\frac{p-p_c}{\sigma}\right)\right] = \frac{2\sqrt{\mathrm{Ln}\,2}}{\sqrt{\pi}\,\sigma}\int_{-\infty}^{p} e^{-4\,(\mathrm{Ln}\,2)\left(\frac{x-p_c}{\sigma}\right)^2} dx \tag{8}$$

The simple form of the first derivative of the model function is helpful to quantitatively characterize the results of different MW methods for various experimental and analytical conditions, for example, dependence of resolution on the window size.

2.2 Autocorrelation Moving-Window (AC-MW) of a Continuous Function

An autocorrelation spectrum can be obtained from the diagonal line of a synchronous 2D correlation map, indicating the intensity variation of each spectral variable over the perturbation range. In autocorrelation moving-window (AC-MW), an autocorrelation spectrum is calculated from each window and the autocorrelation spectra are plotted a 2D contour map of an intensity variation spectrum as a function of the perturbation. For calculation of AC-MW intensity from Eq. 5, a spectral variable is set as $\nu = \nu_1 = \nu_2$, and the integration region is $p_{\mathrm{ave}} - \frac{p_{\mathrm{m}}}{2} < p < p_{\mathrm{ave}} + \frac{p_{\mathrm{m}}}{2}$. Then the mean-centered spectrum, $\tilde{y}(p)$, can be calculated for the spectral variable ν from Eq. 4

$$\tilde{y}(p) = y(p) - \bar{y}(p_{\mathrm{ave}}) = y(p) - \frac{1}{p_m}\int_{p_{\mathrm{ave}}-\frac{p_m}{2}}^{p_{\mathrm{ave}}+\frac{p_m}{2}} y(p)dp \tag{9}$$

where ν is not displayed in $y(p) = y(\nu, p)$ for simplifying the expression. Then, AC-MW intensity $\Phi(p_{\mathrm{ave}})$ can be expressed as

$$\Phi(p_{\mathrm{ave}}) = \Phi(p_{\mathrm{ave}}, \nu) = \frac{1}{p_m}\int_{p_{\mathrm{ave}}-\frac{p_m}{2}}^{p_{\mathrm{ave}}+\frac{p_m}{2}} \tilde{y}(p)^2 dp \tag{10}$$

which is calculated with the model function illustrated in Figure 1b. The functional form of $y(p)$ is shown in Eq. 8 with $p_c = 0$. The $\tilde{y}(p)$ can be analytically expressed from Eq. 9, which can be found as Eq. S1 in the Supplementary Material. The analytical solution of $\Phi(p_{\mathrm{ave}})$ is also calculated from Eq. 10, as shown as Eq. S2 in the Supplementary Material. However, it is not straightforward to recognize similarity or proportionality between the analytical expression of $\Phi(p_{\mathrm{ave}})$ and the first order derivative of $y(p)$.

In order to find quantitative connection between $\Phi(p_{\mathrm{ave}})$ and the first order derivative, the intensity function, $y(p)$ is slightly modified. A narrow section (window) of a slowly varying intensity function can be expressed with a Taylor series of $y(p)$ for the range of $p_{\mathrm{ave}} - \frac{p_{\mathrm{m}}}{2} < p < p_{\mathrm{ave}} + \frac{p_{\mathrm{m}}}{2}$ as,

$$y(p; p_{\mathrm{ave}}) = \sum_{n=0}^{\infty} \frac{y^{(n)}(p_{\mathrm{ave}})}{n!}(p - p_{\mathrm{ave}})^n \tag{11}$$

where $y^{(n)}(p_{\mathrm{ave}})$ is the value of the nth order derivative of $y(p)$ at $p = p_{\mathrm{ave}}$. The polynomials in the Taylor series can be easily calculated for $\tilde{y}(p)$ and $\Phi(p_{\mathrm{ave}})$ in Eqs. 9 and 10, respectively. First, a case is considered that $y(p)$ is approximated to a linear function in Eq. 11, and then,

$$y(p; p_{\mathrm{ave}}) = y(p_{\mathrm{ave}}) + y^{(1)}(p_{\mathrm{ave}})\,(p - p_{\mathrm{ave}}) \tag{12}$$

$$\tilde{y}(p; p_{\mathrm{ave}}) = y(p; p_{\mathrm{ave}}) - \bar{y}(p_{\mathrm{ave}}) = y^{(1)}(p_{\mathrm{ave}})\,(p - p_{\mathrm{ave}}) \tag{13}$$

By inserting Eq. 13 into Eq. 10, the AC-MW intensity is expressed as a simple form

$$\Phi^{(1)}(p_{\mathrm{ave}}) = \left(\frac{p_m^2}{12}\right) \left\{y^{(1)}(p_{\mathrm{ave}})\right\}^2 \tag{14}$$

where the superscript (1) in $\Phi^{(1)}(p_{\mathrm{ave}})$ indicates that the AC-MW intensity is calculated from a linearly approximated $y(p)$ for each moving window. Equation 14 clearly demonstrates that AC-MW intensity becomes proportional to the square of the first derivative *when y(p) can be approximated to a linear function within each moving window*. In other words, when $y(p)$ is curved and the window size is too wide, the shape of $\Phi(p_{\mathrm{ave}})$ will deviate from the square of the first derivative. Equation 14 also shows the quantitative connection between $\Phi^{(1)}(p_{\mathrm{ave}})$ and the square of the first derivative. Therefore, the absolute quantity of $y^{(1)}(p_{\mathrm{ave}})$ can be calculated from $\Phi(p_{\mathrm{ave}})$ when the window size is set to be sufficiently narrow compared with the curvature of $y(p)$.

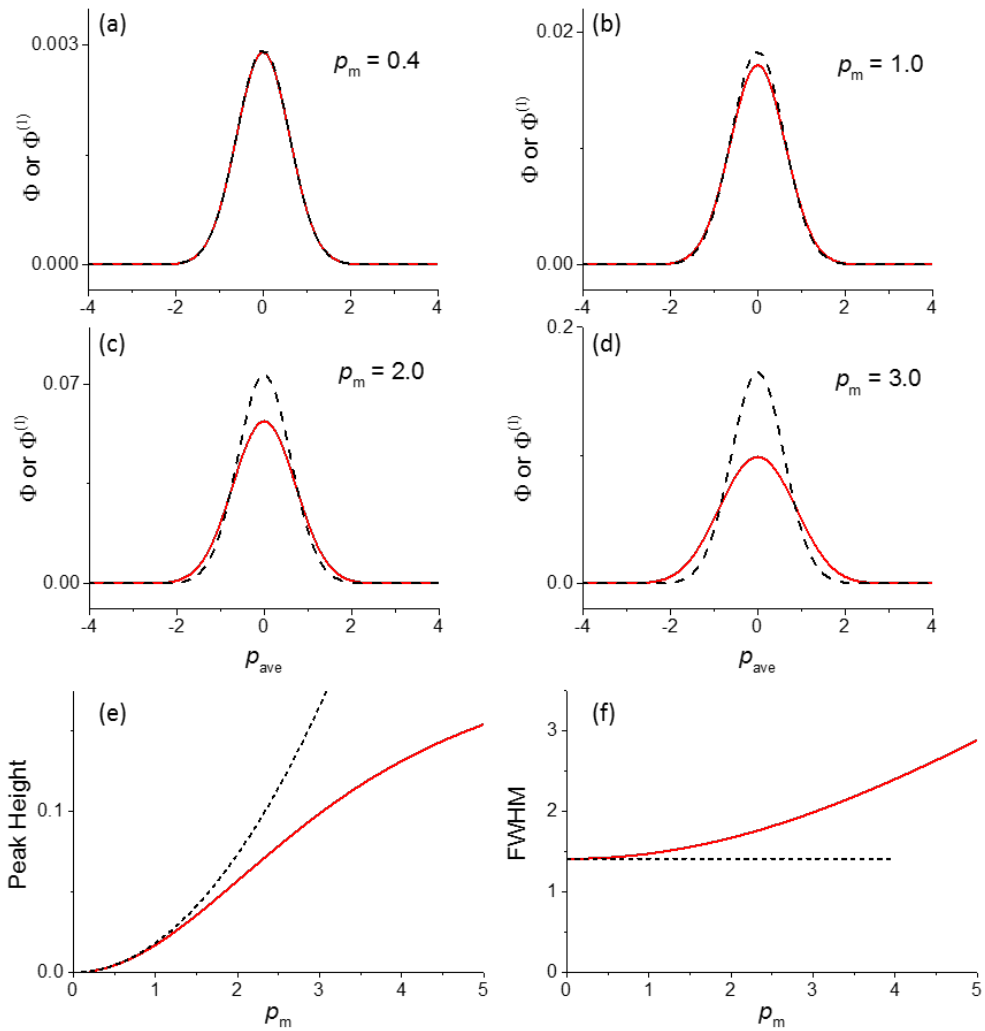

Figure 2. (a) – (d) AC-MW intensity profiles calculated by Eq. 10 for various p_m. The solid red lines indicate $\Phi(p_{ave})$ calculated from the original $y(p)$ of Figure 1b. For comparison, the dashed black lines are $\Phi^{(1)}(p_{ave})$ calculated by Eq. (14) from a linear approximation of $y(p)$ within each moving window. (e) A plot of the peak height of Φ and $\Phi^{(1)}$ as a function of the window size (p_m). (f) A FWHM of the two profiles as a function of p_m. The FWHM of $\Phi^{(1)}$ is constant at $\sqrt{2}$.

Figure 2 shows the $\Phi(p_{ave})$ and $\Phi^{(1)}(p_{ave})$ profiles for four different window sizes and plots of their peak height and FWHM as a function of the window size. First, the $\Phi^{(1)}(p_{ave})$ profiles (the black dotted lines) show the same shape, for different p_m, as the squared $y^{(1)}(p_{ave})$. However, the peak height of $\Phi^{(1)}(p_{ave})$ increases quadratically with p_m, which

is indicated in Eq. 14. By contrast, both the peak height and the FWHM of $\Phi(p_{ave})$, denoted as the red solid lines, are noticeably affected by the window size. As shown in Figure 2e, the peak height of $\Phi(p_{ave})$ becomes smaller than that of $\Phi^{(1)}(p_{ave})$ as the window size becomes larger. The FWHM of $\Phi(p_{ave})$ becomes larger than that of $\Phi^{(1)}(p_{ave})$ (= $\sqrt{\sigma}$). This window-size dependence of $\Phi(p_{ave})$ may be understood as the blurring effect accompanying a moving average used for data smoothing. If the moving-average window size is smaller than the data variation, the smoothed result will be close to the original data. However, if the window size becomes comparable or larger than the data variation, sharp features become smoothed out with lowered intensity and wider width. Based on the data of Figure 2, I would suggest the critical window size $p_m = \sigma/2$, which is a half of the FWHM of the first order derivative. At the critical window size, the relative differences in peak height and FWHM are 7% and 4%, respectively. The suggested criterion of $p_m = \sigma/2$ is good for the model function whose first order derivative is a Gaussian function. A different intensity function may have a different criterion for the appropriate moving window size.

2.3 "Synchronous" Perturbation-Correlation Moving-Window (s-PC-MW) of a Continuous Function

Perturbation-correlation (PC) intensity is calculated by replacing one of the spectral intensity with the perturbation variable in the generalized 2DCOS of Eq. 1 – 4. Similar to the generalized 2DCOS, a generated PC output consists of synchronous and asynchronous correlation intensities, indicating the in-phase and out-of-phase changes of the spectral intensity and the perturbation, respectively. While AC-MW intensity provides information only on the amount of intensity variation, the synchronous perturbation-correlation

moving-window (*s*-PC-MW) intensity determines not only the amount of variation but also the direction of variation. The PC-MW method has been widely used because *s*-PC-MW intensity is assumed to be proportional to the first order derivative of spectral intensity. However, similar to AC-MW, there has been no analytical derivation of those relations and no quantitative characterization of the assumption, to my knowledge. Here is provided an analytical expression for PC-MW intensity by using a continuous function.

The *s*-PC-MW intensity, $\Pi_\Phi(p_{\mathrm{ave}})$, is calculated by replacing $\tilde{y}(\nu_2, p)$ with the mean-centered perturbation, $p - p_{\mathrm{ave}}$, and set the integration range as $p_{\mathrm{ave}} - \frac{p_{\mathrm{m}}}{2} < p < p_{\mathrm{ave}} + \frac{p_{\mathrm{m}}}{2}$ in Eq. 5.

$$\Pi_\Phi(p_{\mathrm{ave}}) = \frac{1}{p_m} \int_{p_{\mathrm{ave}} - \frac{p_{\mathrm{m}}}{2}}^{p_{\mathrm{ave}} + \frac{p_{\mathrm{m}}}{2}} \tilde{y}(p)\ (p - p_{\mathrm{ave}}) dp \tag{15}$$

The model function of Eq. 8 is used for $y(p)$ so that the same expression of the dynamic spectrum from Eq. S1 in the Supplementary Material can be used. From Eq. 15, the analytical expression of $\Pi_\Phi(p_{\mathrm{ave}})$ is obtained and shown as Eq. S3 in the Supplementary Material. Although the expression of $\Pi_\Phi(p_{\mathrm{ave}})$ is simpler than that of $\Phi(p_{\mathrm{ave}})$, it is still not straightforward to find similarity between $\Pi_\Phi(p_{\mathrm{ave}})$ and $y^{(1)}(p_{\mathrm{ave}})$, which is a Gaussian function. Their quantitative connection can be found by approximating $y(p)$ with a linear function from the Taylor series, as used for calculation of $\Phi^{(1)}(p_{\mathrm{ave}})$ in the previous section. $\tilde{y}(p)$ is replaced with the linear function, $y^{(1)}(p_{\mathrm{ave}})\ (p - p_{\mathrm{ave}})$, in Eq. 15, and then the *s*-PC-MW intensity is expressed in a simple analytical form,

$$\Pi_\Phi^{(1)}(p_{\mathrm{ave}}) = \left(\frac{p_m^2}{12}\right)\ y^{(1)}(p_{\mathrm{ave}}) \tag{16}$$

As for $\Phi^{(1)}(p_{\mathrm{ave}})$, the superscript (1) in $\Pi_\Phi^{(1)}(p_{\mathrm{ave}})$ indicates the *s*-PC-MW intensity is calculated from a linearly approximated function for each moving window. Equation 16

suggests that *s*-PC-MW intensity becomes proportional to the first derivative *when y(p) can be approximated to a linear function within each moving window*. It also suggests that the absolute quantity of $y^{(1)}(p_{\mathrm{ave}})$ can be determined from a calculated $\Pi_{\Phi}(p_{\mathrm{ave}})/\left(\frac{p_m^2}{12}\right)$ value if the window size is set to be sufficiently narrow compared with the curvature of *y*(*p*).

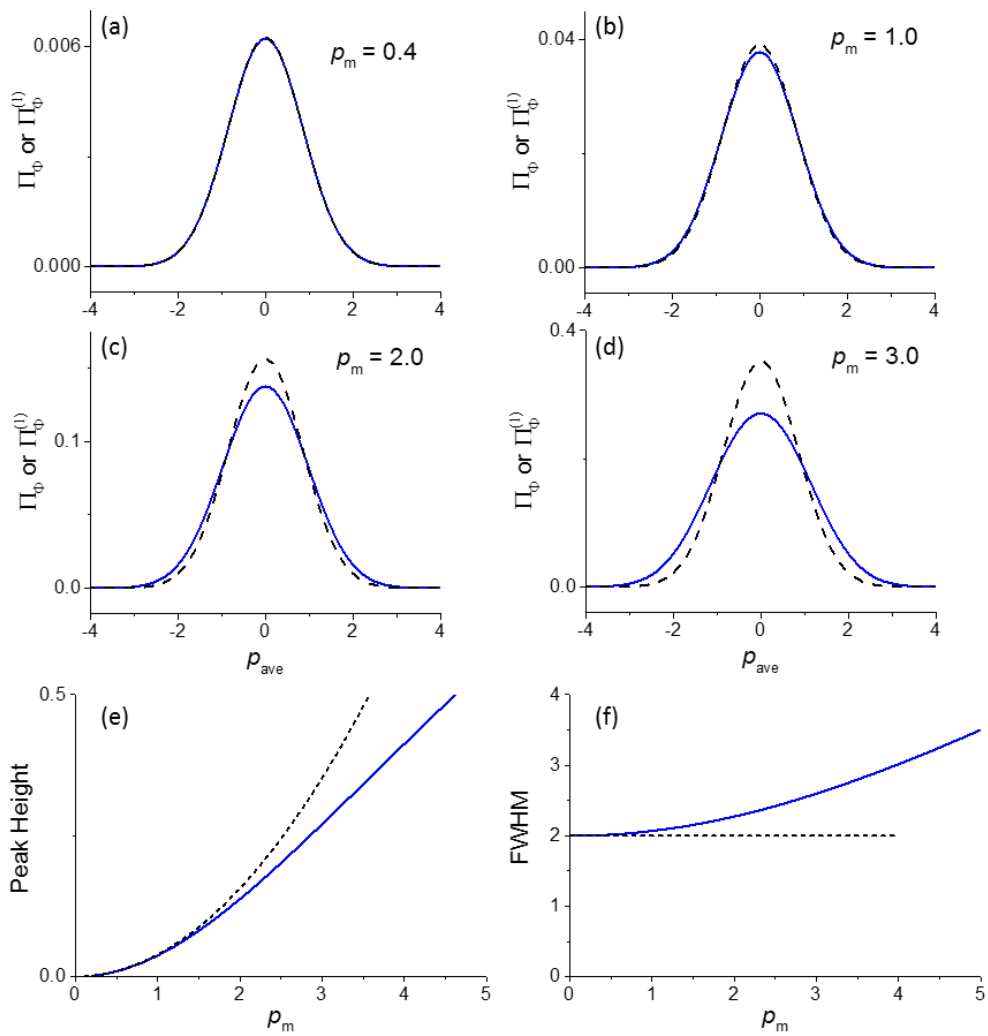

Figure 3. (a) – (d) Synchronous PC-MW (*s-PC*-MW) intensity profiles calculated by Eq. 15 for various p_{m}. The solid blue lines indicate $\Pi_{\Phi}(p_{\mathrm{ave}})$ calculated by using the original *y*(*p*) of Figure 1b. For comparison, the dashed black lines are $\Pi_{\Phi}^{(1)}(p_{\mathrm{ave}})$, calculated by Eq. 16 from a linear

approximation of $y(p)$ within each moving window. (e) A plot of peak height of Π_Φ and $\Pi_\Phi^{(1)}$ as a function of p_m. (f) A FWHM of the two profiles as a function of p_m. The FWHM of $\Pi_\Phi^{(1)}$ is constant at 2.

Figures 3a–3d show the $\Pi_\Phi(p_{ave})$ and $\Pi_\Phi^{(1)}(p_{ave})$ intensity profiles for different p_m. Overall, the window size effect on *s*-PC-MW is similar to those on AC-MW. When the window size is small, $\Pi_\Phi(p_{ave})$ is close to $\Pi_\Phi^{(1)}(p_{ave})$, which is proportional to $y^{(1)}(p_{ave})$. However, as the window size becomes larger, the peak height of $\Pi_\Phi(p_{ave})$ becomes smaller than that of $\Pi_\Phi^{(1)}(p_{ave})$, and the FWHM becomes larger than that of $\Pi_\Phi^{(1)}(p_{ave})$. For *s*-PC-MW, I suggest the same critical window size as AC-MW, $p_m = \sigma/2$, leaving relative differences in peak height and FWHM between Π_Φ and $\Pi_\Phi^{(1)}$ as 3% and 3%, respectively.

2.4 "Asynchronous" Perturbation-Correlation Moving-Window (as-PC-MW) of a Continuous Function

Asynchronous PC-MW (*as*-PC-MW) is the out-of-phase term of PC-MW, as complementary to synchronous PC-MW (*s*-PC-MW). The calculation of *as*-PC-MW is similar to that of *s*-PC-MW: $\tilde{y}(\nu_2, p)$ is replaced with the mean-centered perturbation, $p - p_{ave}$, and the integration range is set as $p_{ave} - \frac{p_m}{2} < p < p_{ave} + \frac{p_m}{2}$ in the generalized 2DCOS formulae of Eqs. 6 and 7. An additional required step is to calculate $\mathbf{H}(p - p_{ave})$, which is the Hilbert transform of $(p - p_{ave})$. The analytical form of *as*-PC-MW intensity is expressed as

$$\Pi_\Psi(p_{ave}) = \frac{1}{p_m}\int_{p_{ave}-\frac{p_m}{2}}^{p_{ave}+\frac{p_m}{2}} \tilde{y}(p)\mathcal{H}(p - p_{ave})dp \tag{17}$$

By substituting p with $(x + p_{ave})$, Eq. 17 is simplified as

$$\Pi_{\Psi}(p_{\mathrm{ave}}) = \frac{1}{p_m}\int_{-\frac{p_{\mathrm{m}}}{2}}^{\frac{p_{\mathrm{m}}}{2}} \tilde{y}(x + p_{\mathrm{ave}})\mathcal{H}(x)dx \tag{18}$$

and

$$\mathcal{H}(x) = \frac{1}{\pi} PV \int_{-\frac{p_{\mathrm{m}}}{2}}^{\frac{p_{\mathrm{m}}}{2}} \frac{p}{p-x} dp = \frac{1}{\pi}\left\{p_m + x \ \mathrm{Ln}\left(\frac{p_m - 2x}{p_m + 2x}\right)\right\} \tag{19}$$

Calculation with the model function of Eq. 8 for $y(p)$ yields the analytical expression of $\Pi_{\Psi}(p_{\mathrm{ave}})$, as shown in Eq. S4 in the Supplementary Material. The expression is complex as it includes the Cauchy principal value to exclude the singularity from $\mathcal{H}(x)$. As used for $\Phi(p_{\mathrm{ave}})$ and $\Pi_{\Phi}(p_{\mathrm{ave}})$ in the previous sections, $\tilde{y}(p)$ is replaced with the linear function, $y^{(1)}(p_{\mathrm{ave}})\ (p - p_{\mathrm{ave}})$, in Eq. 18 and find that $\Pi_{\Psi}^{(1)}(p_{\mathrm{ave}}) = 0$. This can be explained by the fact that $\tilde{y}(x + p_{\mathrm{ave}}) = x$ is an odd function while $\mathcal{H}(x)$ is an even function in Eq. 18 and that integration of the product of the odd function and the even function over $-\frac{p_{\mathrm{m}}}{2} < x < \frac{p_{\mathrm{m}}}{2}$ becomes zero. Therefore, a second order truncated Taylor series is used for $\tilde{y}(p)$ as

$$y(x + p_{\mathrm{ave}}) = y(p_{\mathrm{ave}}) + y^{(1)}(p_{\mathrm{ave}})\ x + \frac{y^{(2)}(p_{\mathrm{ave}})}{2}\ x^2 \tag{20}$$

where $y^{(2)}(p_{\mathrm{ave}})$ is the second order derivative of $y(p)$ at $p = p_{\mathrm{ave}}$. The mean-centered spectrum becomes from Eq. 9

$$\tilde{y}(x + p_{\mathrm{ave}}) = -\frac{p_m^2 y^{(2)}(p_{\mathrm{ave}})}{24} + y^{(1)}(p_{\mathrm{ave}})\ x + \frac{y^{(2)}(p_{\mathrm{ave}})}{2}\ x^2 \tag{21}$$

By inserting Eqs. 19 and 21 into Eq. 18,

$$\Pi_{\Psi}^{(2)}(p_{\mathrm{ave}}) = -\frac{{p_m}^3}{48\pi} y^{(2)}(p_{\mathrm{ave}}) \tag{22}$$

The superscript (2) in $\Pi_{\Psi}^{(2)}(p_{\mathrm{ave}})$ indicates the *as*-PC-MW intensity is calculated from a quadratically approximated function for each moving window. Equation 22 shows that the

as-PC-MW intensity is proportional to the negative of $y^{(2)}(p_{\mathrm{ave}})$, which is consistent with the previous simulation-based study[9], *when y(p) can be approximated to a quadratic function within each moving window*. In addition, it confirms that the sign of $\Pi_{\Psi}(p_{\mathrm{ave}})$ means the direction of the curvature of $y(p)$: $\Pi_{\Psi}(p_{\mathrm{ave}}) > 0$ is for convex-upward (or concave-downward), and $\Pi_{\Psi}(p_{\mathrm{ave}}) < 0$, for convex-downward (or concave upward).

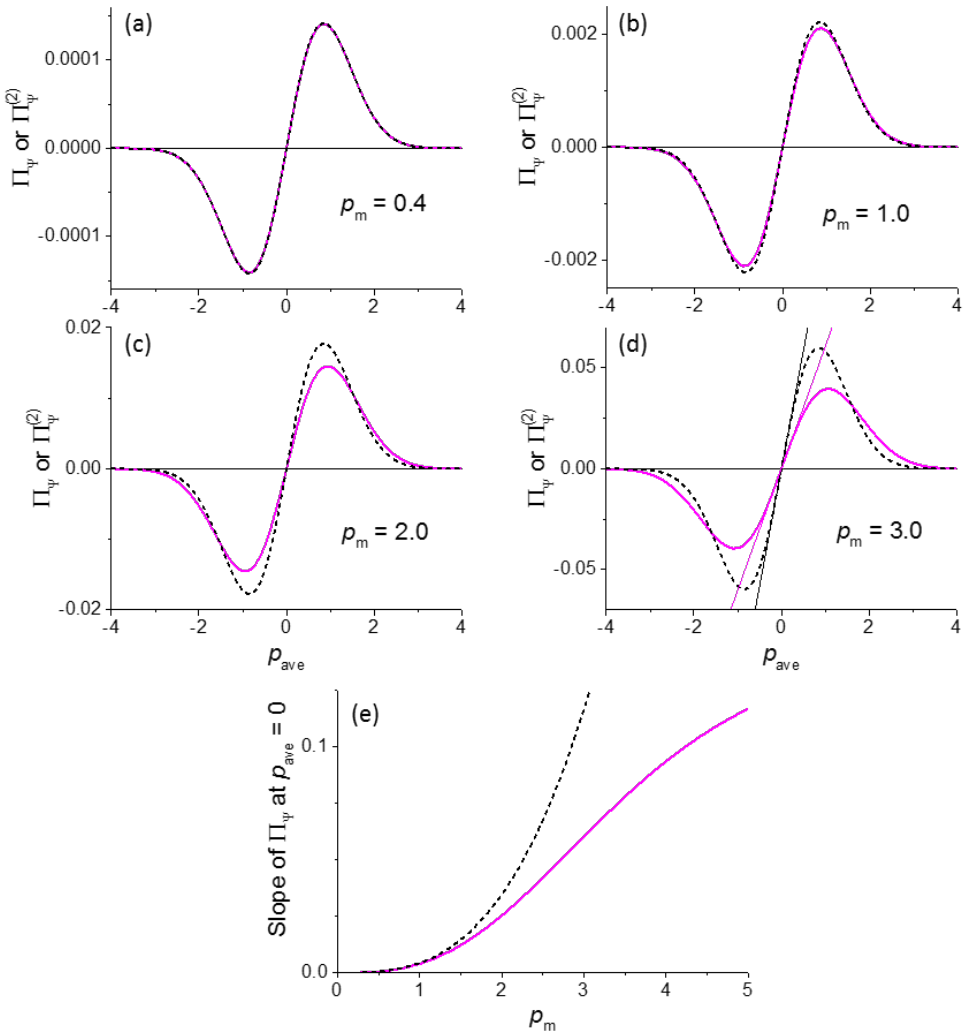

Figure 4. (a) – (d) Asynchronous PC-MW (*as-PC*-MW) intensity profiles calculated by Eq. 18 for various p_m. The solid magenta lines indicate $\Pi_{\Psi}(p_{\mathrm{ave}})$ calculated from the original $y(p)$ of Figure 1b. For comparison, the dashed black lines are $\Pi_{\Psi}^{(2)}(p_{\mathrm{ave}})$ calculated by Eq. 22 from the second-order truncated Taylor series of $y(p)$. (e) The slopes of Π_{Ψ} and $\Pi_{\Psi}^{(2)}$ at $p_{\mathrm{ave}} = 0$ are plotted as a function of p_m.

Figures 4a–4d show the $\Pi_\Psi(p_{\mathrm{ave}})$ and $\Pi_\Psi^{(2)}(p_{\mathrm{ave}})$ intensity profiles for different p_{m}. Similar to the AC-MW and *s*-PC-MW results, when the window size is small, $\Pi_\Psi(p_{\mathrm{ave}})$ is close to $\Pi_\Psi^{(2)}(p_{\mathrm{ave}})$. However, as window size increases, $\Pi_\Psi(p_{\mathrm{ave}})$ begins to deviate from $\Pi_\Psi^{(2)}(p_{\mathrm{ave}})$. Unlike AC-MW and *s*-PC-MW, *as*-PC-MW is an odd function about the symmetry center ($p_{\mathrm{ave}} = 0$). Therefore, instead of peak height or FWHM, the slope of the tangential line of $\Pi_\Psi(p_{\mathrm{ave}})$ and $\Pi_\Psi^{(2)}(p_{\mathrm{ave}})$ at the symmetry center is used for comparison, as shown in Figure 4e. The slopes of $\Pi_\Psi(p_{\mathrm{ave}})$ are very close to that of $\Pi_\Psi^{(2)}(p_{\mathrm{ave}})$ for small window size but becomes lower as window size increases. Again, as a criterion for quantitative equivalency between Π_Ψ and $\Pi_\Psi^{(2)}$, I suggest the window size p_{m} be smaller than $\sigma/2$ for the intensity function of Eq. 8, where the relative difference in the slope of the tangential line is 8%.

3. Numerical Descriptions of Moving-Window Correlation Spectroscopy

The previous section discusses the characteristics of various MW methods and their physical implications by using integrals of a continuous model function for the spectral intensity as a function of perturbation. The general characteristics observed from calculation of a continuous function include the window size effect on peak intensity and bandwidth of the calculated MW profiles and the equivalency of AC-MW, *s*-PC-MW, and *as*-PC-MW profiles to $\{y^{(1)}\}^2$, $y^{(1)}$, and $y^{(2)}$, respectively. In actual experimental measurements, however, spectral intensity data are not acquired as a *continuous* function of perturbation. Instead, they are acquired in the *discrete* form of perturbation. Although

the general characteristics of MW analysis results from a discrete-perturbation spectral data will represent those from its equivalent continuous-perturbation spectral function, some practical parameters are uniquely applicable to measurements and analyses of a discrete form of experimental data. This section examines the effect of those discrete-specific parameters on each MW result by using a set of simulation data.

3.1 Moving-Window 2D Correlation of Discrete Data

Numerical methods of MW correlation spectroscopy for discrete forms of spectral data are basically the same as the formulations used for continuous analytical functions in the previous section. Simply, the integrals used for continuous functions are to be replaced with numerical integrations or summations for a finite set of discrete data, and the basic formulation for MW correlation intensity has been introduced in many publications.[9,19,20] Briefly, spectral intensity $y(p_j)$ is measured at a discrete perturbation variable p_j. A moving window can be defined for a subset of $(2m+1)$ spectra of $y(p_J)$, where $j - m \leq J \leq j + m$. The perturbation p_J's are assumed to be uniformly spaced, until differently stated later. Then, the mean-centered spectrum can be expressed in a similar form to Eq. 9,

$$\tilde{y}(p_J) = y(p_J) - \bar{y}(p_j) = y(p_J) - \frac{1}{2m+1}\sum_{J=j-m}^{j+m} y(p_J) \tag{23}$$

and the mean-centered perturbation is expressed

$$\tilde{p}_J = p_J - \bar{p}_J = p_J - p_j \tag{24}$$

where p_j is the average perturbation of the moving window.

Similarly, numerical integration for uniformly spaced p_J can convert an integral form of MW intensity into a simple summation form. For example, AC-MW intensity $\Phi(p_j)$ can be expressed from Eq. 10

$$\Phi(p_j) = \frac{1}{2m+1}\sum_{J=j-m}^{j+m}\tilde{y}(p_J)^2 \tag{25}$$

Similarly, *s*-PC-MW intensity $\Pi_\Phi(p_j)$ can be converted from Eq. (15) into

$$\Pi_\Phi(p_j) = \frac{1}{2m+1}\sum_{J=j-m}^{j+m}\tilde{y}(p_J)\tilde{p}_J \tag{26}$$

However, *as*-PC-MW intensity requires additional complicated steps to be calculated in a summation form due to the Hilbert-transformation, $\mathcal{H}(p - p_{\mathrm{ave}})$, in Eq. (17). However, Noda simplified the transformation by introducing a simple matrix, called the discrete Hilbert-Noda transformation matrix,

$$M_{JK} = \begin{cases} 0 & J = K \\ \frac{1}{\pi(K-J)} & J \neq K \end{cases} \tag{27}$$

Then, $\Pi_\Phi(p_j)$ can be expressed in a simple form

$$\Pi_\Psi(p_j) = \frac{1}{2m+1}\sum_{J=j-m}^{j+m}\tilde{y}(p_J)\sum_{K=j-m}^{j+m}M_{JK}\,\tilde{p}_K \tag{28}$$

First the square root of AC-MW intensity ($\sqrt{\Phi}$), and *s*-PC-MW intensity (Π_Φ) are compared as their analytical functions are proportional to the first order derivative of an intensity function when the window size is sufficiently small. For uniformly spaced data, the window size is constant and defined as the product of the perturbation increment and the number of data per window. For numerical comparison between $\sqrt{\Phi}$ and Π_Φ, the same model function as in Figure 1b is used to generate a discrete intensity data $y(p_j)$. Calculated $\sqrt{\Phi}$ and Π_Φ, from Eqs. 25 and 26, respectively, are normalized by their maximum intensities for shape comparison.

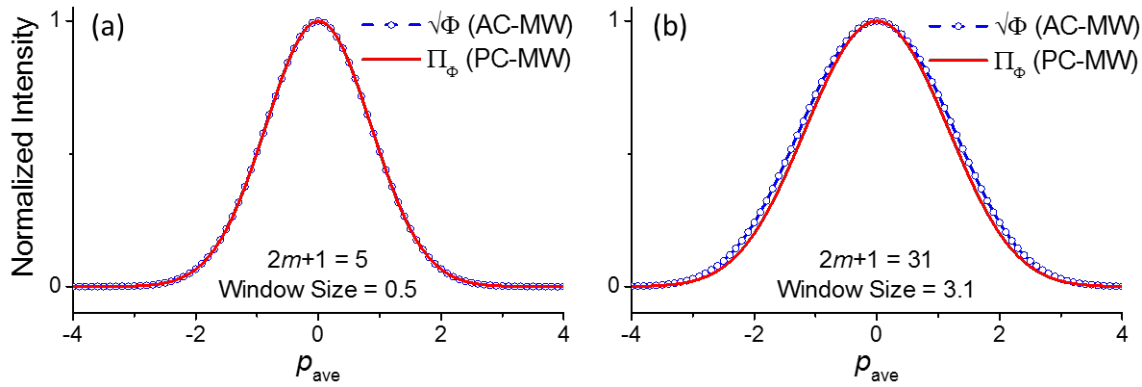

Figure 5. Comparisons of normalized profiles of the square root of AC-MW ($\sqrt{\Phi}$) and *s*-PC-MW (Π_Φ). The intensity data are generated from the intensity function of Eq. 8 with $p_c = 0$ and $\sigma = 2$, with an increment of 0.1. (a) Results of $\sqrt{\Phi}$ and Π_Φ calculated with $2m + 1 = 5$. The FWHMs measured from the generated profiles are 2.02 and 2.00 for $\sqrt{\Phi}$ and Π_Φ, respectively. (b) Results of $\sqrt{\Phi}$ and Π_Φ calculated with $2m + 1 = 31$. The measured FWHMs are 2.83 and 2.65 for $\sqrt{\Phi}$ and Π_Φ, respectively.

Figure 5 shows the normalized curves of $\sqrt{\Phi}$ and Π_Φ calculated for two different window sizes. First, in Figure 5a, when the moving window size is smaller than the FWHM of the model function, both normalized profiles are almost indistinguishable, and their apparent FWHMs are close to the value of σ (= 2). By contrast, in Figure 5b, when the moving window size is larger than the bandwidth of the model function, the FWHM of both profiles become wider than σ. The $\sqrt{\Phi}$ curve becomes even wider than the Π_Φ curve. This result reconfirms that two MW methods can be considered equivalent as a metric of the first order derivative as long as the window size is narrower than the FWHM of $y^{(1)}$.

3.3 Effects of non-uniform spacing of perturbations on AC-MW, s-PC-MW, and as-PC-MW

So far numerical expressions of AC-MW, *s*-PC-MW, and *as*-PC-MW of Eqs. 23 – 28 are based on the condition that perturbation variables are uniformly spaced. All MW correlation intensity calculations shown in previous publications, to my knowledge, are based on the same assumption of uniform perturbation spacing. In real experiments, however, it is often extremely challenging to acquire spectral data at perfectly uniformly spaced perturbations. For example, temperatures monitored while a series of spectra are measured can be easily different from the set temperatures for various reasons including imperfect temperature controller or inherent system fluctuation. In some experimental conditions, perturbation increment has to be varied monotonically during measurements. A proper consideration of non-uniform perturbation increments can be found in the conversion from integration of Eqs. 10, 15, and 18 to numerical summation of Eqs. 25, 26, and 28. Each increment ($p_{J+1} - p_J$) or ($p_J - p_{J-1}$) must be multiplied to the term in the summation and the denominator ($2m + 1$) must be replaced by ($p_{j+m} - p_{j-m}$). In addition, the average perturbation is no longer p_j and needs to be calculated separately for the mean-centering process before the summation. To circumvent the complication due to non-uniform spacing in numerical integration, one can generate uniformly spaced data by interpolating the original non-uniformly spaced data. However, this data manipulation can cause unwanted bias in analysis and error propagation due to imperfect interpolation models and incorrect weighting. Here, both MW intensities are calculated from a set of simulation data with either uniform and non-uniform perturbation spacing.

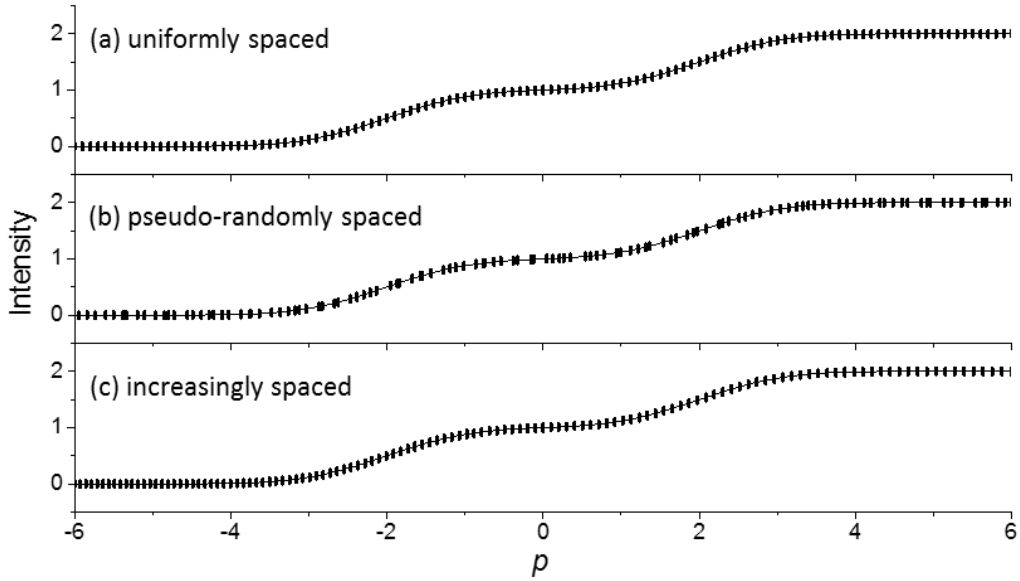

Figure 6. Simulated discrete intensity data with three different types of perturbation spacing. The intensity function $y(p)$ is defined by Eq. 29, where the FWHM σ is set to be 2. (a) Perturbation increments are uniformly spaced as 0.1. (b) Perturbation increments are pseudo-randomly spaced with the average spacing of 0.1 added by a random number generated in the range between –0.05 and +0.05. (c) Perturbation increments are increasingly spaced. The increment increases linearly from 0.072 (at p = –6) to 0.122 (at p = 6). At p = 0, the increment is 0.1, which is the same as (a).

First, three types of perturbation arrays are generated: one with uniform spacing, another with pseudo-randomly fluctuating increments, and the other with monotonically increasing increments. Then, corresponding spectral intensities are calculated with a model function,

$$y(p) = \frac{1}{2}\mathrm{erfc}\left[-2\sqrt{\mathrm{Ln}\,2}\,\left(\frac{p-2}{\sigma}\right)\right] + \frac{1}{2}\mathrm{erfc}\left[-2\sqrt{\mathrm{Ln}\,2}\,\left(\frac{p+2}{\sigma}\right)\right] \tag{29}$$

which is the sum of two identical functions with differently shifted p_c from Eq. 8. This two-peaked model function makes it easier to understand non-uniform spacing effects than a single-peak function. Figure 6 shows the three simulation data with different types of perturbation spacing. It must be noted that for all three perturbation arrays the

corresponding spectral intensity $y(p_j)$ is calculated with the identical model function without any intensity noise.

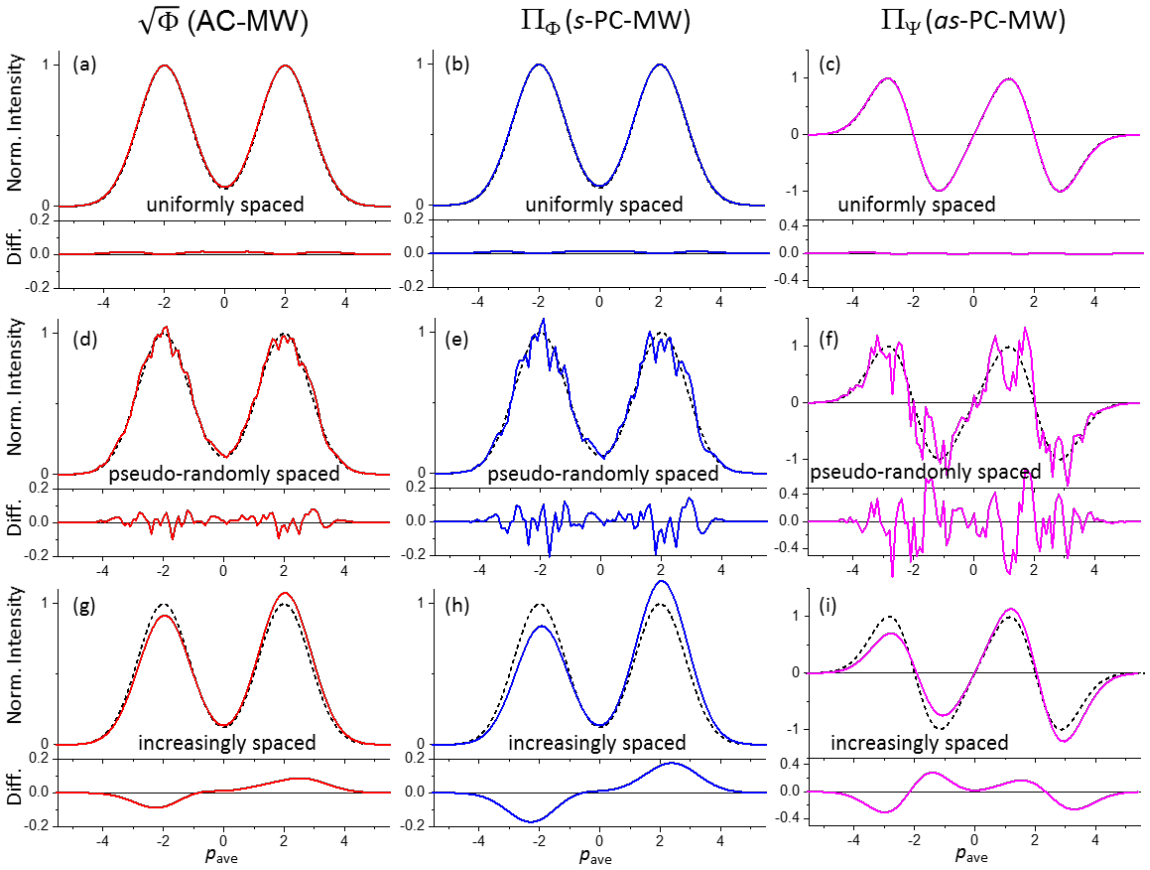

Figure 7. Effects of non-uniform perturbation spacing on the square root of AC-MW, *s*-PC-MW, and *as*-PC-MW. The simulation data sets of Figure 6 are used for calculation. For all calculations, the same number of spectra per window, $2m + 1 = 7$ is used. The actual window size varies depending on the spacing types. For the uniform spacing on the top row, the window size is constant at 0.7. For the pseudo-random spacing, the window size varies randomly between 0.66 and 0.73. For the increasing spacing on the bottom row, the window size increases monotonically from 0.55 (at $p_{ave} = -5.5$) to 0.82 (at $p_{ave} = 5.5$). The peak height of the MW profile calculated from the uniformly spaced perturbation data is used to normalize the MW profiles from the other perturbation spacing types. The differences of $\sqrt{\Phi}$ and Π_Φ are calculated by subtracting them with the normalized first order derivative of the model intensity function, which is plotted together as the dashed lines. The difference of Π_Φ is calculated by subtracting them with the normalized second order derivative of the model intensity function, which is also plotted together as the dashed lines.

Figure 7 shows results of $\sqrt{\Phi}$, Π_Φ, and Π_Ψ calculated from the identical simulation data with the three types of perturbation spacing (uniform, pseudo-random, and increasing). For all calculations in Figure 7, the number of spectra per window ($2m + 1$) is set to be seven so that its corresponding window size is smaller than $\sigma/2$ (= 1.0) for all three types of perturbation spacing. For the data with uniformly spaced perturbation, $\sqrt{\Phi}$ and Π_Φ are very similar to the first order derivative function, as already shown in Figure 5a. By contrast, $\sqrt{\Phi}$ and Π_Φ calculated from the pseudo-randomly spaced perturbations are quite different from those from the uniformly spaced perturbations. Both $\sqrt{\Phi}$ and Π_Φ show noticeable fluctuations around the peak regions. The amount of fluctuation of the Π_Φ profile is as large as 10% of the peak intensities while that of $\sqrt{\Phi}$ is even larger and as large as 20% of the peak intensities. The effect of non-uniform spacing is much greater on Π_Ψ than on $\sqrt{\Phi}$ and Π_Φ (note that the *y*-scale of Π_Ψ difference is different from that of $\sqrt{\Phi}$ and Π_Φ).

Figures 7g–7i show the profiles of $\sqrt{\Phi}$, Π_Φ, and Π_Ψ of the data with increasingly spaced perturbations. Similar to the case of pseudo-randomly spaced perturbation data, $\sqrt{\Phi}$, Π_Φ, and Π_Ψ all show a very strong dependence on the increment spacing. It must be noted that because window size of the increasingly spaced perturbation in Figures 7g–7i is smaller than that of the uniformly spaced perturbation in Figures 7a–7c for $p < 0$ and larger for $p > 0$. This strong window size dependence of $\sqrt{\Phi}$ and Π_Φ is not straightforwardly recognizable in their numerical integration formula of Eqs. 25, 26, and 28. Instead, this window size dependence of $\sqrt{\Phi}$, Π_Φ, and Π_Ψ can be found in the corresponding analytical

expressions calculated from a linearly or quadratically truncated Taylor series for $y(p)$. Equations 14, 16, and 22 shows that $\sqrt{\Phi^{(1)}} \propto p_m$, $\Pi_{\Phi}^{(1)} \propto {p_m}^2$, and $\Pi_{\Psi}^{(1)} \propto {p_m}^3$, which are consistent with the window size effects shown in the difference profiles of Figures 7g–7i. The inherent window size dependence of AC-MW and PC-MW correlation intensities causes the unwanted fluctuation and distortion in the observed values of $\sqrt{\Phi}$, Π_{Φ}, and Π_{Ψ}. If one wants to use $\sqrt{\Phi}$, Π_{Φ}, and Π_{Ψ} as metrics for the first or second order derivative of the spectral intensity measured with non-uniform perturbation increments, one needs to calculate a Riemann sum or other appropriate numerical integration of each moving window and scale it with its corresponding window size.

3.4 Effects of noise in spectral intensity on AC-MW and PC-MW

Experimentally measured spectral intensity data do contain various types of noises. Previously, Morita et al. characterized intensity noise effect on AC-MW with introducing random noise to simulation data.[19] Here the effect of intensity noise on the three MW methods is examined when two types of noise contributions to spectral intensity are considered: one is intensity-independent noise, such as dark noise and CCD readout noise; and the other is intensity-dependent noise, such as shot noise. The two types of noise contributions are considered as

$$y^{\text{noise}}(p) = y(p) + \mathbf{RN}(u) + \mathbf{RN}(v\sqrt{y(p)}) \tag{30}$$

where $\mathbf{RN}(u)$ denotes the random number generation function between $-u$ and $+u$ for $u \geq 0$. The second term and the third term on the right hand side of Eq. 30 indicate intensity-independent and intensity-dependent noise contributions, respectively. For a simple

analysis, perturbation increments are set to be uniformly spaced, and the window size is also set to be smaller than the half of the bandwidth of the intensity function.

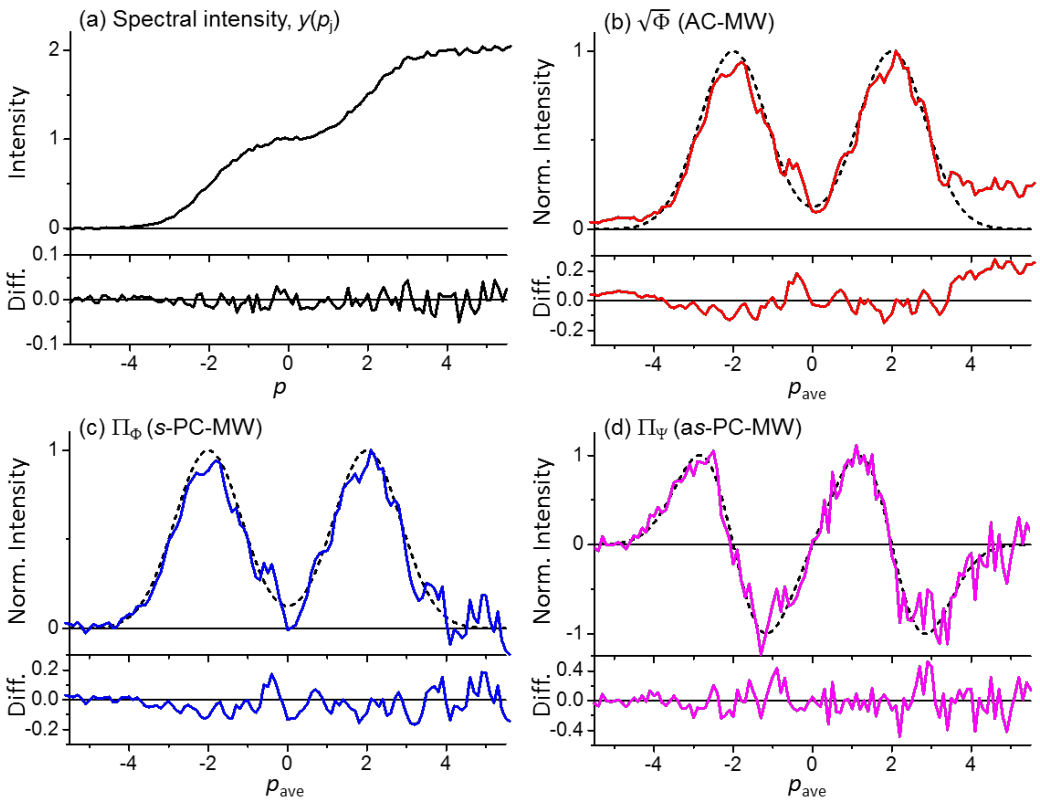

Figure 8. (a) Spectral intensity $y(p_j)$ added with two types of noises defined in Eq. 30 with $u = 0.01$ for intensity-independent noise and $v = 0.02$ for intensity-dependent noise. The difference plot is calculated between the noise-added intensity and the noise-free intensity. (b) The square root of AC-MW ($\sqrt{\Phi}$), (c) *s*-PC-MW (Π_Φ), and (d) *as*-PC-MW (Π_Ψ) profiles are calculated with the noise-added intensity (solid lines) and the noise-free intensity (dotted lines). The perturbation increments are constant at 0.1, and $2m + 1 = 7$. for Both MW correlation plots from the noise-added and noise-free intensity are normalized by the maximum MW correlation intensity value from the noise-free intensity. The difference plot is calculated between the MW correlation intensity from the noise-added and noise-free intensity.

Figure 8 shows the noise-added spectral intensity and the calculated MW correlation intensity from the spectral intensity. When the intensity is low ($p < -4$), it is

contributed by only intensity-independent noise. As the intensity increases, the noise becomes larger due to both intensity-independent noise and intensity-dependent noise. Similarly, the calculated MW correlation intensities show larger intensity fluctuation where intensity noise is larger. Interestingly, the AC-MW ($\sqrt{\Phi}$) result shows different characteristics from the PC-MW (Π_Φ and Π_Ψ) results in response to intensity noise. In Figures 8c and 8d, the fluctuating Π_Φ and Π_Ψ curves calculated from the noise-added intensity, on average, follows the corresponding Π_Φ curve from the noise-free intensity. By contrast, the $\sqrt{\Phi}$ intensity falls into only the positive side and shows offset drifts from the corresponding $\sqrt{\Phi}$ curve from the noise-free intensity where $\sqrt{\Phi}$ intensity is close to zero ($p < -4$ and $p > 4$). The positive offset drift is larger where spectral intensity fluctuation is larger at $p > 4$. The offset drift of $\sqrt{\Phi}$ is explained by the square term of mean-centered spectral intensity, $\tilde{y}(p_J)^2$, in the summation of Eq. 25. This offset drift in a $\sqrt{\Phi}$ plot is potentially misleading as false peaks in data interpretation.

The three MW analysis results are characterized for discrete simulation data with different types of perturbation spacing and with different types of intensity noise. All three MW correlation intensities are affected by perturbation spacing and the corresponding window size variation. In addition, AC-MW intensity is found to show offset drift due to intensity noise.

4. Conclusion

Analytical and numerical expressions of autocorrelation MW (AC-MW), synchronous perturbation-correlation MW (*s*-PC-MW), and asynchronous perturbation-correlation MW (*as*-PC-MW) have been described. The square root of AC-MW and *s*-PC-

MW can be approximated to be proportional to the first order derivative when moving-window size is sufficiently narrow compared with the bandwidth of spectral change. Also, *as*-PC-MW can represent the second order derivative when window size is sufficiently narrow. For discrete spectral data, non-uniform perturbation increment can cause undesired fluctuation or distortion in all three MW intensity profiles. Intensity noise can cause an offset drift in AC-MW intensity, which can mislead interpretation. This analytical and numerical characterization of those widely used MW correlation intensities clarifies their physical meanings and explains their appropriate analytical conditions.

AUTHOR INFORMATION

E-mail: youngjong.lee@nist.gov

DISCLAIMER

Official contribution of the National Institute of Standards and Technology; not subject to copyright in the United States.

REFERENCES

1. I. Noda. “Generalized two-dimensional correlation method applicable to infrared, Raman, and other types of spectroscopy”. Appl. Spectrosc. 1993. 47(9): 1329–1336.

2. I. Noda, Y. Ozaki. Two-Dimensional Correlation Spectroscopy. Wiley & Sons, Chichester, West Sussex, 2004.

3. M. Thomas, H.H. Richardson. “Two-dimensional FT-IR correlation analysis of the phase transitions in a liquid crystal, 4′-n-octyl-4-cyanobiphenyl (8CB)”. Vib. Spectrosc. 2000. 24(1): 137–146.

4. S. Šašić, Y. Katsumoto, H. Sato, Y. Ozaki. “Applications of Moving Window Two-Dimensional Correlation Spectroscopy to Analysis of Phase Transitions and Spectra Classification”. Anal. Chem. 2003. 75(16): 4010–4018.

5. Y. Jin, A.P. Kotula, A.R. Hight Walker, K.B. Migler, Y.J. Lee. “Phase-specific Raman analysis of n -alkane melting by moving-window two-dimensional correlation spectroscopy”. J. Raman Spectrosc. 2016. 47(11): 1375–1384.

6. L. Peng, T. Zhou, Y. Huang, L. Jiang, Y. Dan. “Microdynamics mechanism of thermal-induced hydrogel network destruction of poly(vinyl alcohol) in D2O studied by two-dimensional infrared correlation spectroscopy”. J. Phys. Chem. B. 2014. 118(31): 9496–9506.

7. A.N.L. Batista, J.M. Batista, L. Ashton, V.S. Bolzani, M. Furlan, E.W. Blanch. “Investigation of DMSO-Induced Conformational Transitions in Human Serum Albumin Using Two-Dimensional Raman Optical Activity Spectroscopy”. Chirality. 2014. 26(9): 497–501.

8. L. Ashton, E.W. Blanch. “pH-induced conformational transitions in a-lactalbumin investigated with two-dimensional Raman correlation variance plots and moving windows”. J. Mol. Struct. 2010. 974(1–3): 132–138.

9. S. Morita, H. Shinzawa, I. Noda, Y. Ozaki. “Perturbation-Correlation Moving-Window Two-Dimensional Correlation Spectroscopy”. Appl. Spectrosc. 2006.

60(4): 398–406.

10. A. Watanabe, S. Morita, Y. Ozaki. “Study on temperature-dependent changes in hydrogen bonds in cellulose Iβ by infrared spectroscopy with perturbation-correlation moving-window two-dimensional correlation spectroscopy”. Biomacromolecules. 2006. 7(11): 3164–3170.

11. R. Gomez De La Cuesta, R. Goodacre, L. Ashton. “Monitoring antibody aggregation in early drug development using raman spectroscopy and perturbation-correlation moving windows”. Anal. Chem. 2014. 86(22): 11133–11140.

12. T. Nishii, S. Morita, T. Genkawa, M. Watari, D. Ishikawa, Y. Ozaki. “Moving-window two-dimensional heterospectral (MW2DHetero) correlation analysis and its application for the process monitoring of alcoholic fermentation”. Appl. Spectrosc. 2015. 69(6): 665–670.

13. Z. Ye, Y. Li, Z. An, P. Wu. “Exploration of Doubly Thermal Phase Transition Process of PDEGA- b -PDMA- b -PVCL in Water”. Langmuir. 2016. 32: 6691−6700.

14. C. Li, J. Liu, J. Li, F. Shen, Q. Huang, H. Xu. “Studies of 4,4′-diphenylmethane diisocyanate (MDI)/1,4-butanediol (BDO) based TPUs by in situ and moving-window two-dimensional correlation infrared spectroscopy: Understanding of multiple DSC endotherms from intermolecular interactions and motions level”. Polymer. 2012. 53(23): 5423–5435.

15. Y. Chen, T. Mu. “A new way to interpret perturbation-correlation moving-window two-dimensional correlation spectroscopy: probing the dynamic interaction of ionic liquid 1-ethyl-3-methylimidazolium acetate to absorb atmospheric water.” Appl. Spectrosc. 2015. 69(1): 130–42.

16. M. Unger, S. Morita, H. Sato, Y. Ozaki, H.W. Siesler. “Variable-Temperature Fourier Transform Infrared Spectroscopic Investigations of Poly (3-Hydroxyalkanoates) and Perturbation-Correlation Moving-Window Two-Dimensional Correlation Analysis. Part I : Study of Non-Annealed and Annealed Poly (3-Hydroxybutyrate) Homopolymer”. Appl. Spectrosc. 2009. 63(9): 1027–

1033.

17. S.R. Ryu, I. Noda, C.H. Lee, P.H. Lee, H. Hwang, Y.M. Jung. “Two-dimensional correlation analysis and waterfall plots for detecting positional fluctuations of spectral changes”. Appl. Spectrosc. 2011. 65(4): 359–368.

18. Y.M. Jung, H.S. Shin, S. Bin Kim, I. Noda. “Two-Dimensional Gradient Mapping Technique Useful for Detailed Spectral Analysis of Polymer Transition Temperatures”. J. Phys. Chem. B. 2008. 112(12): 3611–3616.

19. S. Morita, H. Shinzawa, R. Tsenkova, I. Noda, Y. Ozaki. “Computational simulations and a practical application of moving-window two-dimensional correlation spectroscopy”. J. Mol. Struct. 2006. 799(1–3): 111–120.

20. H. Shinzawa, S. Morita, I. Noda, Y. Ozaki. “Effect of the window size in moving-window two-dimensional correlation analysis”. J. Mol. Struct. 2006. 799(1–3): 28–33.

21. S. Morita, H. Shinzawa, I. Noda, Y. Ozaki. “Effect of band position shift on moving-window two-dimensional correlation spectroscopy”. J. Mol. Struct. 2006. 799: 16–22.

22. T. Zhou, L. Peng, Y. Liu, Y. Zhan, F. Liu, A. Zhang. “An insight into the sequential order in 2D correlation spectroscopy using polymer transitions: Boltzmann Sigmoid, Gaussian Cumulative, Lorentz Cumulative, and Asymmetric Sigmoid. Findings in experiments and simulations”. Vib. Spectrosc. 2014. 70: 137–161.

23. I. Noda. “Determination of two-dimensional correlation spectra using the Hilbert transform”. Appl. Spectrosc. 2000. 54(7): 994–998.